CHAPTER 5

HEAT TRANSFER ENHANCEMENT IN AIR COOLING WITH VORTEX GENERATOR

5.1 Introduction

At present, electronic circuits have been designed to have smaller sizes and more functions. The power densities contained in a printed circuit board increases thus the thermal control is highly emphasized to keep the the temperature of the electronic equipment not exceed the designed temperature to ensure the system reliability and its performance.

There are many techniques for the thermal management and the convective air cooling is still the most common because of its low maintenance and low investment. However, the common forced air cooling is not sufficient in case of high power dissipation, especially, for the complex electronic components.

Fiebig (1998) point out that there are three major heat transfer enhancement mechanisms of enhanced surfaces, namely: (1) developing boundary layers, (2) swirl or vortices, and (3) flow destabilization or turbulence intensification.

Though interrupted surface can significantly improve the heat transfer performance, the associated penalty of pressure drop is also tremendous. In contrast to the common interrupted surfaces, the vortex generator not only improves the heat transfer performance but also reveals comparatively small pressure drops. This is because wall friction is related to the derivative of streamwise velocity but not spanwise and normal velocities. The vortex generator characterized the secondary flow pattern from the vertical motion that is caused by the spanwise and normal velocities. Heat transfer enhancement is associated with the secondary flow but with small penalty of wall friction (Jacobi and Shah, 1995). Therefore, longitudinal vortices are recognized especially suitable for heat transfer applications.

Heat transfer enhancement of air cooling by vortex generator is one passive method that generates streamwise vortices which creates high turbulence in fluid flow over heat transfer surfaces. Delta winglet vortex generator is one of the promising tecniques to integrate in compact heat exchangers and shows a very good heat transfer performance. Wrobleski and Eibeck(1991) showed that the longitudinal vortices imbedded into turbulent boundary layers and enhanced the heat transfer. Fiebig et al., (1986) and Fiebig(1998) had studied the influences of different types of vortex generators on heat transfer performance such as delta wing, rectangular winglet , and delta winglet and the best performance is the delta winglet type. Fiebig et al., (1993) also used vortex-induced device in finned tube banks and they found that the heat transfer coefficient increased by 55 – 65 % for in-line tube arrangement and by 9 % for staggered arrangement. The corresponding pressure drop was increased by 20 – 45 % and 3 %, respectively. Kwak et al., (2003) also studied the heat transfer and pressure loss penalty of stagged finned –tube bundles with delta winglet pairs set in the front row of the tube bundle at low Reynolds number(350-2100) and better heat transfer performance was also taken.

Vortex generators have also been applied to enhance heat transfer in electronic modules. Garimella and Eibeck (1991) investigated heat transfer enhancement by installing a row of half-delta wing vortex generators upstream of a heated copper chip array. The study used water as coolant and two heights of the vortex generators (one and two times of the chip height) are considered. The maximum heat transfer enhancement were found at the second row. The significant heat transfer enhancement was found in laminar region and the addition effect due to the vortex generator was rather small in turbulent zone. The pressure across the array was found to be close to that without the vortex generators. Higher the generator height also gave better thermal performance. Jubran and Al-Salaymeh (1999) studied thermal wake and pressure drop characteristics in a set of electronic modules when there were different shape and sizes of ribs fixed to the array board. The thermal wake function of the chips downstream could be reduced significantly.

The present study aims to experimentally investigate the heat transfer performance and the pressure drop of electronic modules with the presence of delta winglet vortex generator integrated in front of all electronic modules. The electronic modules are arranged in in-line and staggered arrays.

5.2 Experimental Procedure

The experiments are performed in a small wind turbine with a test section as shown in Figure 5.1. The air flow rate could be controlled and the height of the air channel could be adjusted. There is a flow straightener to keep a uniform airflow before entering the test section.

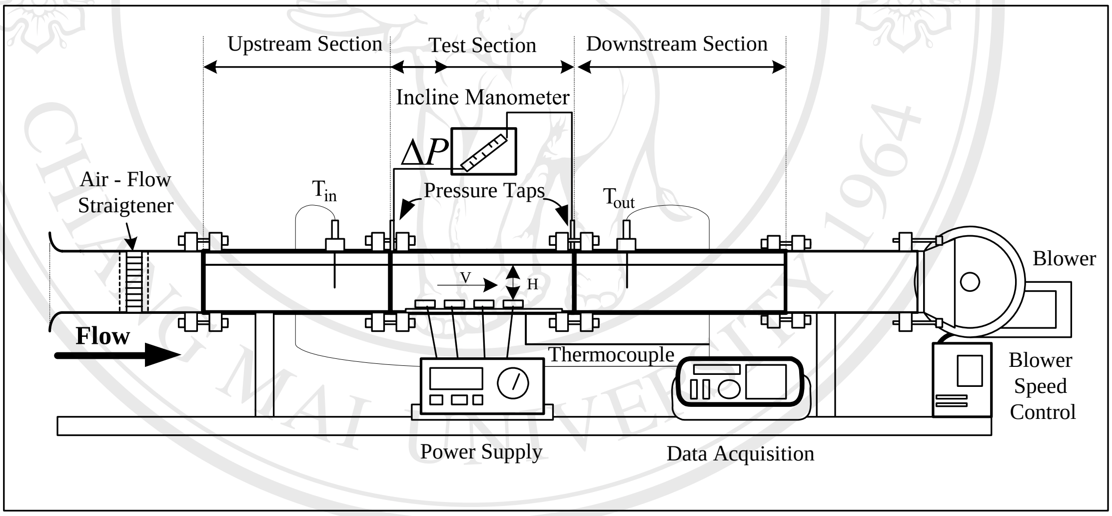

Figure 5.1 The wind tunnel for the experimental test.

The chip modules in the study are artificial elements each of 1.8 cm x 5.8 cm x 0.6 cm having an electrical foil-heater inside. The chip dimensions are similar to those of the real 64 pins electronic chip. The artificial chip surface is polished aluminum surface thus the radiation effect could be neglected (Rodgers et al., 2003). There is an insulating tape between the module and the epoxy board and the epoxy board is also insulated at the back thus the heat conduction to the board is rather small. The modules are arranged in in-line and staggered arrays and fixed to a printed circuit board of which the back is well insulated. The delta winglet vortex generators similar to that given in Figure 5.2, for in-line and staggered arrays, are also integrated into the board as shown in Figure 5.3. The temperatures of the chips and the inlet air temperature are measured by a set of K-type thermocouples having ±0.1°C accuracy, the rate of heat generated in each chip is read directly from a wattmeter with ±0.1 W accuracy and the air inlet velocity are monitored by a hot wire anemometer with ±0.1 m/s accuracy. The data at steady-state conditions are used to derive the heat transfer coefficients and the thermal wake function. The experimental test conditions are given in Table 5.1.

Table 5.1

The test conditions (In-line array).

Variables	values
Re_H	3600 / 5400 / 7200 / 9000
H_{cw}	0.018 m
B	0.006 m
L_X	0.058 m
L_Y	0.018 m
C_X	0.019 m / 0.038 m
C_Y	0.018 m
B_X	0.0420 m
B_Y	0.0160 m
VG_H	0.012 m
VG_L	0.021 m
α	10 / 20 degree
q_k	5 W/module
$k_{(PCB),Epoxy}$	2 W/mK
T_o	27 ^{0}C

The test conditions (Staggered array).

Variables	**values**
Re_H	3400 / 5100 / 6800
H_{ww}	0.024 m
B	0.006 m
L_X	0.058 m
L_Y	0.018 m
C_X	0.019 m
C_Y	0.018 m(D1) / 0.036 m / 0.054 m(D2)
B_X	0.0420 m
B_Y	0.0160 m(D1) / 0.025 m(D2)
VG_H	0.012 m
VG_L	0.021 m
α	20 degree
q_k	2.5 W/module
$k_{(PCB),Epoxy}$	2 W/mK
T_o	27 ^{0}C

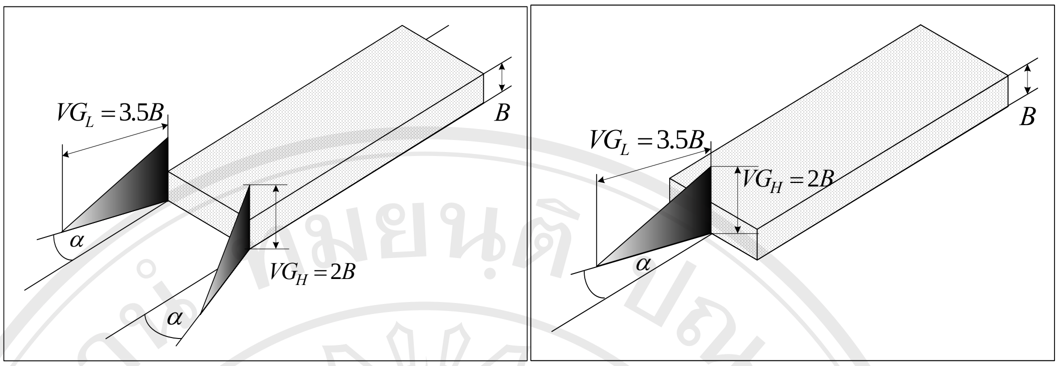

(a) In-line array. (b) Staggered array.

Figure 2 The delta winglet vortex generators.

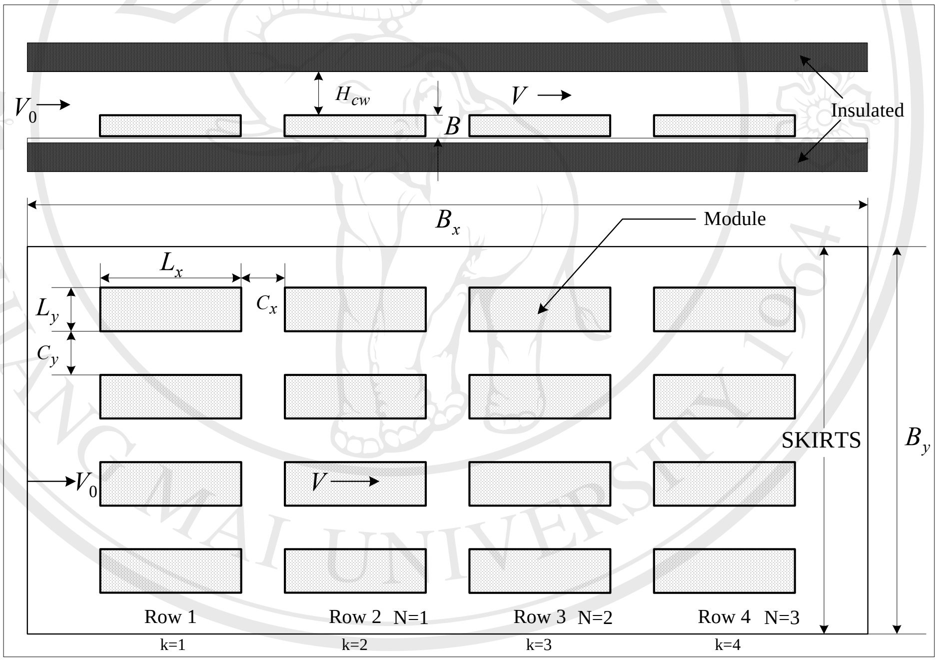

(a) In-line arrangement.

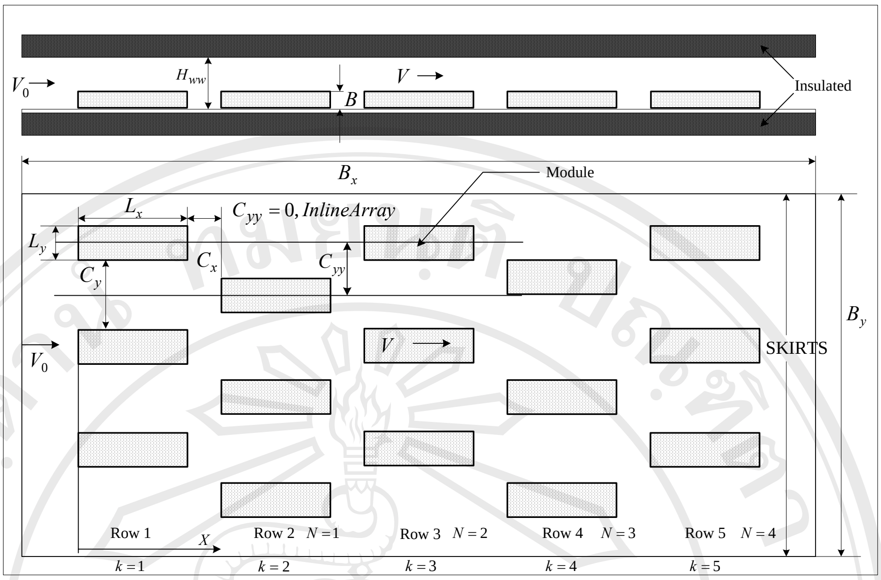

(b) Staggered arrangement. The chip density is D where $D = \dfrac{L_X L_Y}{(L_X + C_X)(L_Y + C_Y)}$.

Figure 5.3 Configurations of the winglet vortex generators on the circuit board.

5.3. Data Reduction

In this part, another method looked like a superposition technique to evaluate the temperatures of the modules. The temperature rise in electronic module, for convective effect, comes from its heat generation and thermal wake which results to heat release from the upstream components. When the thermal radiation effect is neglected, the temperature rise in each electronic chip could be calculated by (Arvizu and Moffat, 1982).

$$T_k - T_0 = \left(\frac{q_k}{h_k A_k}\right) + \sum_{i=1}^{k-1} \theta_{k-i}\left(T_i - T_0\right), i < k \,. \tag{5.1}$$

q_k is the internal heat generation in the k_{th} chip, A_k is the heat transfer area and h_k is adiabatic heat transfer coefficient which could be calculated from

$$h_k = \frac{q_k}{A_k (T_k - T_0)}\Bigg|\, only q_k \neq 0 \,. \tag{5.2}$$

θ_k is thermal wake function which is the fraction temperature increase of the k^{th} component due to heat release from the other elements. The function could be calculated by

$$\theta_{k-i} = \frac{T_k - T_0}{T_i - T_0}\bigg|_{q_i \neq 0, q_k = 0}. \tag{5.3}$$

5.4. Experimental Results

5.4.1 In-line Array

5.4.1.1 Adiabatic Heat Transfer Coefficient

***(a)* No vortex generators**

Figure 5.4 shows the adiabatic heat transfer coefficient in term of adiabatic Nusselt number at different positions of the chip modules in in-line array compared with those of the other researcher (Anderson and Moffat, 1990) when there is no vortex generator. It could be seen that the value when the ratio X/D_h around 6(starting from the third row) is nearly constant which means that the fully developed in convection process is obtained (Wirtz, 1996) and the values of the leading rows (rows 1-3) are in the entrance region. Figure 5.5 shows the comparison of the adiabatic heat transfer coefficient at the third row compared with the literature data under the fully developed condition. It could be seen that the present results agree well with those of the previous studies in both regions.

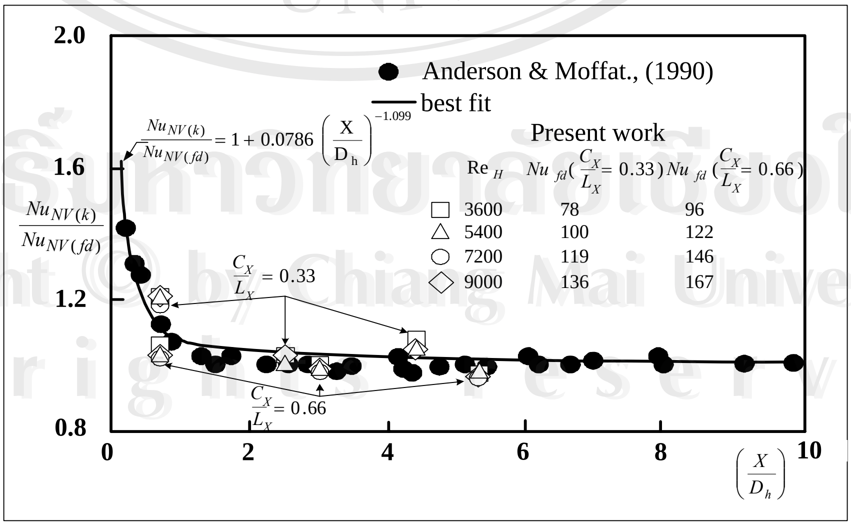

Figure 5.4 The adiabatic heat transfer coefficient of each row of the in-line module at different positions in entrance region. No vortex generator is integrated.

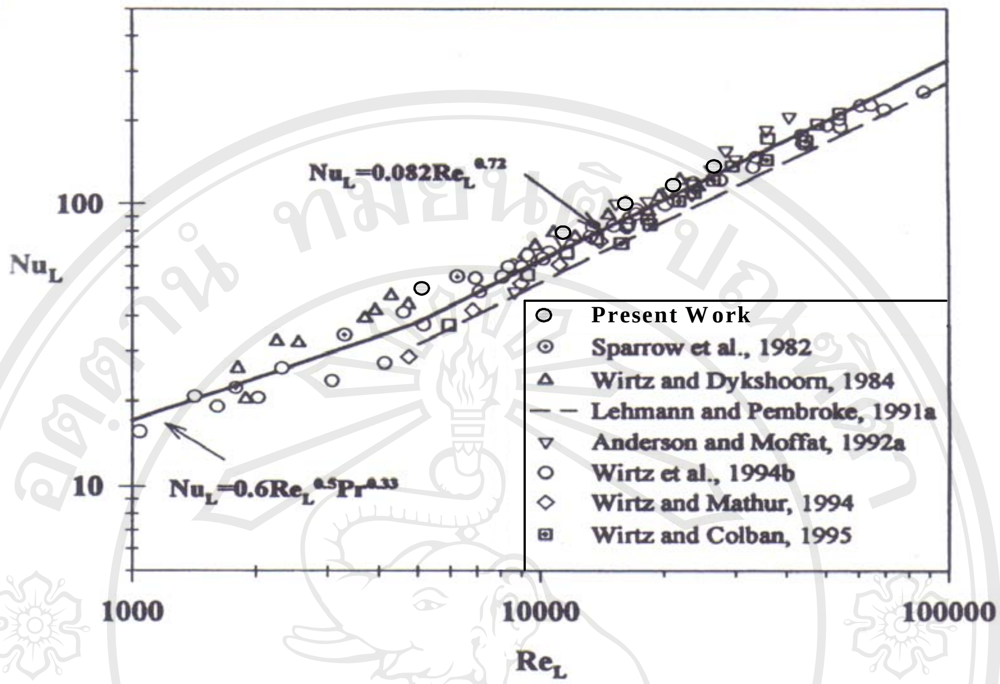

Figure 5.5 Comparison of the fully developed adiabatic heat transfer coefficient for the in-line module array when $C_X/L_X=0.33$ with the literature data. No vortex generator is integrated.

From Figures 5.4 and 5.5 the Nusselt number could be set as

Entrance region: $$\frac{Nu_{NV(k)}}{Nu_{NV(fd)}} = 1 + 0.0786\left(\frac{X}{D_h}\right)^{-1.099} \quad (5.4)$$

Fully developed region: $$Nu_{NV(fd)} = 0.3434\,\mathrm{Re}_H{}^{0.607}\left(\frac{H_{cw}}{L_X}\right)^{-0.670}\left(\frac{C_X}{L_X}\right)^{0.295} \quad (5.5)$$

It could be seen that the second row get the poorest heat transfer coefficient followed by the third row because there is a recirculation perpendicular to the secondary air flow exists in the inter-block gaps. The last chip heat transfer coefficient is higher than those of the second and the third elements because the air could move more freely.

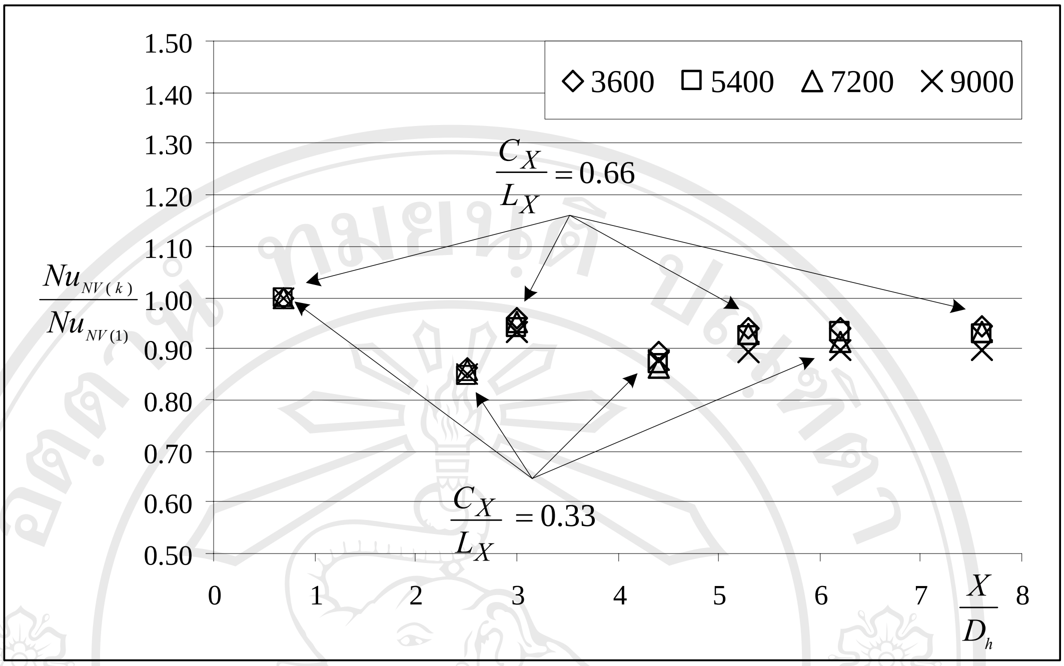

Figure 5.6 The ratio of adiabatic Nusselt number at different positions to that at the first row at various values of $\frac{X}{D_h}$. No vortex generator.

Figure 5.6 shows the ratio of adiabatic Nusselt number at different positions to that at the first row at various values of X/D_h when there is no vortex generator integrated. From the figure, it could be seen that the value of Reynolds number slightly affect on the ratio of the Nusselt number at different positions to that at the first row. For the entrance region (row 1 to row 3), a correlation could be performed as

$$\frac{Nu_{NV(k)}}{Nu_{NV(1)}} = 1.2141\mathrm{Re}^{-0.018236}\left(\frac{C_X}{L_X}\right)^{0.08321}\left(\frac{X}{D_h}\right)^{-0.058644} \quad (5.6)$$

The correlation gives ± 6 % error from the experimental data.

(b) With vortex generators

Figure 5.7 shows the adiabatic heat transfer coefficients when there are vortex generators with different attack angles integrated in front of all chip modules. It could be seen that the longitudinal vortices are performed in the fluid flow by the vortex generators then the heat transfer coefficients in all rows could be increased more than the previous case especially at the second row. The Reynolds number does not give a strong effect to the heat transfer augmentation. It could also be found that the generator having higher attack angle gives better heat transfer enhancement. The angle is not recommended to be over 20^{o} because it will block the flow and create high pressure drop.

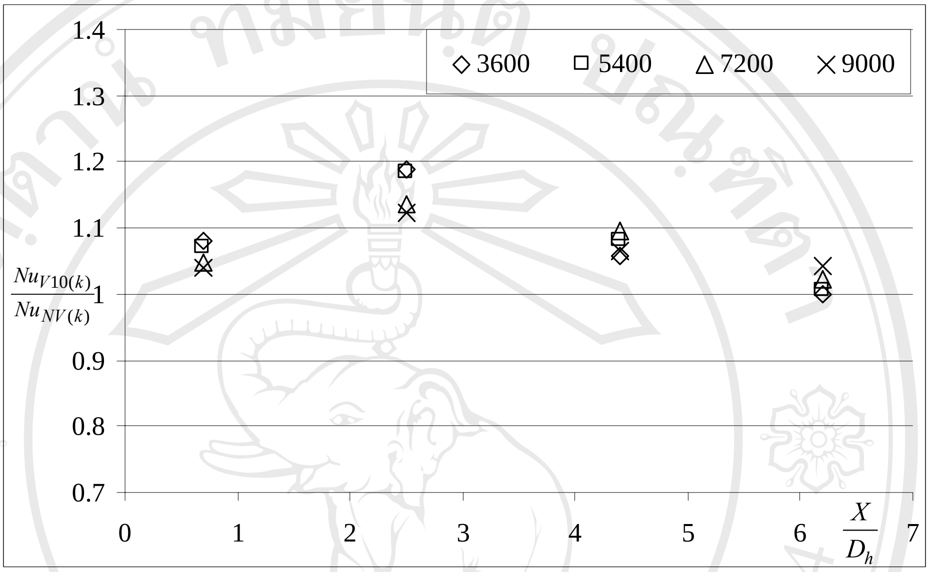

(a) Attack angle 10 degree.

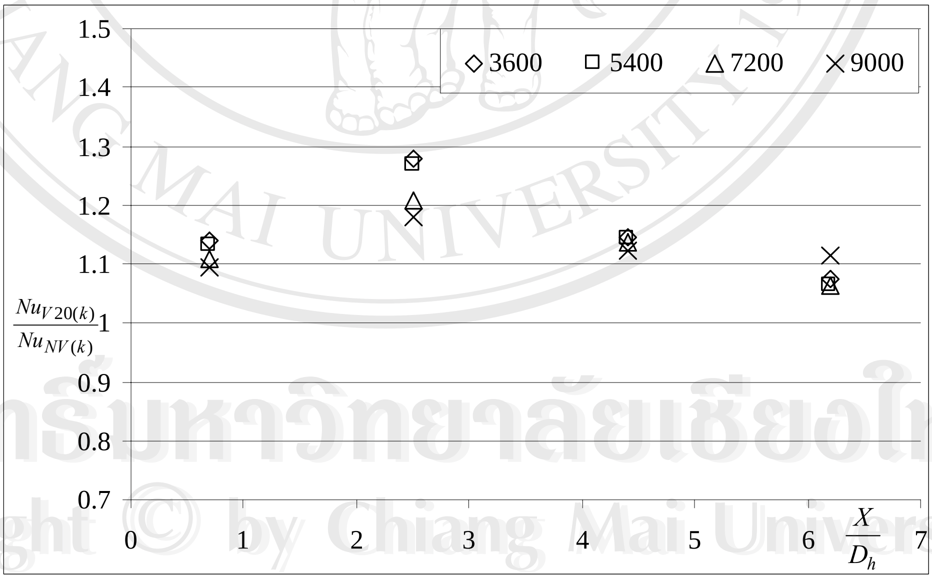

(b) Attack angle 20 degree.

Figure 5.7 The heat transfer enhancement in term of Nusselt numbers with and without vortex generators. The vortex generators are integrated in front of all modules. The attack angles are 10 and 20 degree.

Figure 5.8 also shows the ratio of adiabatic Nusselt numbers at different positions and different attack angles with that at the first row. The parameters could be correlated as

$$\frac{Nu_{V(k)}}{Nu_{V(1)}} = 1.0732\,\mathrm{Re}^{-0.01032}\left(\frac{X}{D_h}\right)^{-0.06194}\tan\alpha^{0.0022051} \quad (5.7)$$

The correlation gives ± 5 % error from the experimental data.

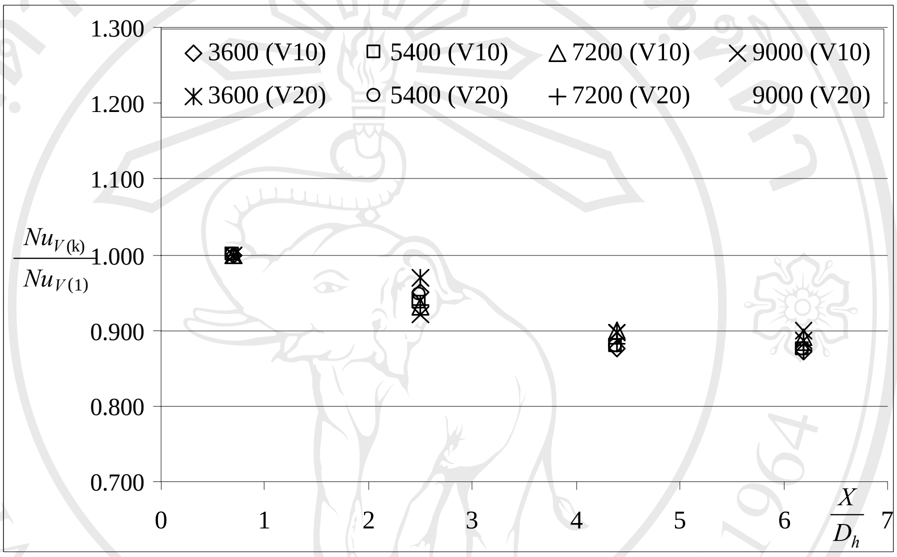

Figure 5.8 The ratio of adiabatic Nusselt numbers at different postitions to that at the first row at various values of X/D_h and different attack angles. There is a set of vortex generators integrated in front of all modules.

A correlation between the Nusselt numbers in the first row (with and without vortex generator) and Reynolds number is given as

$$\frac{Nu_{V(1)}}{Nu_{NV(1)}} = 1.591\,\mathrm{Re}^{-0.04454}\tan\alpha^{0.04496} \quad (5.8)$$

The correlation gives ± 3 % from the experimental data. The results are also given in Figure 5.9.

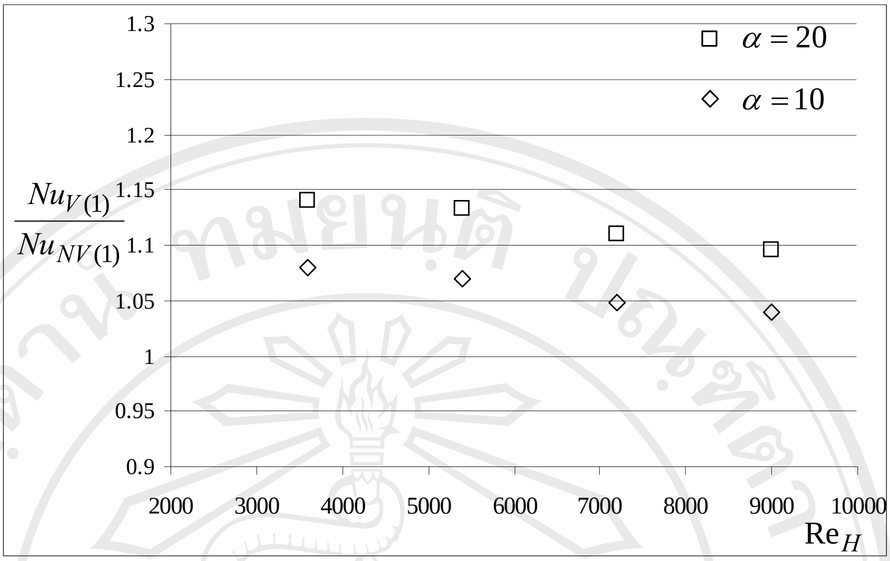

Figure 5.9 The ratio of adiabatic Nusselt numbers with and without vortex generator for the first row at various values of Reynolds number. There is a set of vortex generators integrated in front of all modules.

From the above correlations, the adiabatic Nusselt number of the modules with integrated vortex generators could be evaluated from that without the vortex generator as

$$\frac{Nu_{V(k)}}{Nu_{NV(k)}} = \left(\frac{Nu_{V(k)}}{Nu_{V(1)}}\right) \times \left(\frac{Nu_{V(1)}}{Nu_{NV(1)}}\right) \times \left(\frac{Nu_{NV(1)}}{Nu_{NV(k)}}\right) \tag{5.9}$$

Our experiments when a set of vortex generators are installed only in front of the first row are also carried out. The results are shown in Fig. 5.10. The chip modules at the first row only get a strong effect of the longitudinal flow compared with those without the vortex generators thus high heat transfer enhancement is obtained. The vortex generators slightly enhance the heat transfer in the next rows therefore this arrangement is not concentrated in this study.

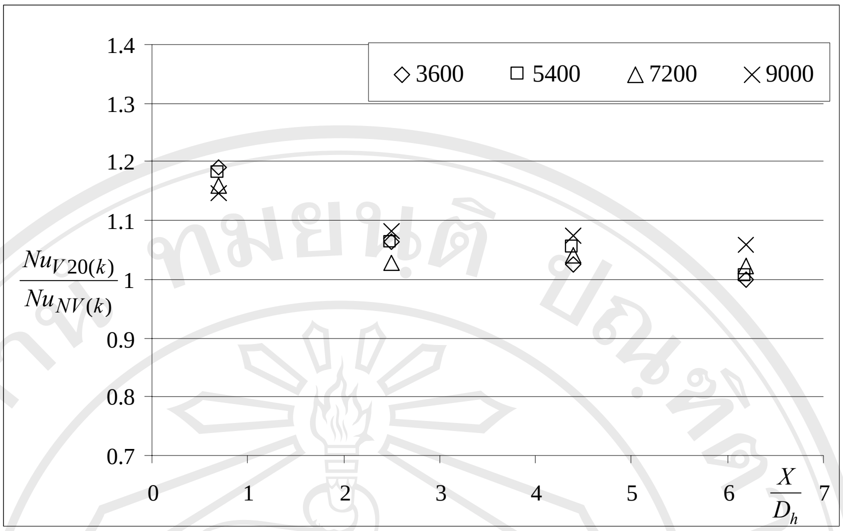

Figure 5.10 The heat transfer enhancement in term of adiabatic Nusselt Numbers with and without vortex generators. The vortex generators are integrated in front of the first row only. The attack angle is 20 degree.

5.4.1.2 Thermal Wake Function

(a) No vortex generator

When one row of electronic modules is heated, the temperatures of the modules downstream will also get this heating result which is called the thermal wake effect. Figure 5.11 shows the results of thermal wake function of the module immediately downstream from the first heating module when there is no vortex generator. Figure 5.12 shows the thermal wake functions for other downstream modules. It could be seen that the thermal wake functions of the modules are similar to that described by Fagri et al.,(1996) and Jubran and Al-Salaymeh(1999) of which the correlations of the thermal wake functions are

$$\frac{\theta_{NV(N)}}{\theta_{NV(1)}} = 0.20756\,\mathrm{Re}^{0.17935}\,N^{-0.76936} \qquad (5.10)$$

where

$$\theta_{NV(1)} = 3.7091\mathrm{Re}_H^{-0.3653} \qquad (5.11)$$

The correlation gives ± 10 % from the experimental data.

An example of the calculation at Re_H = 5400 compared to the data of Jubran and Al-Salaymeh(1999) is also shown in Figure 5.13.

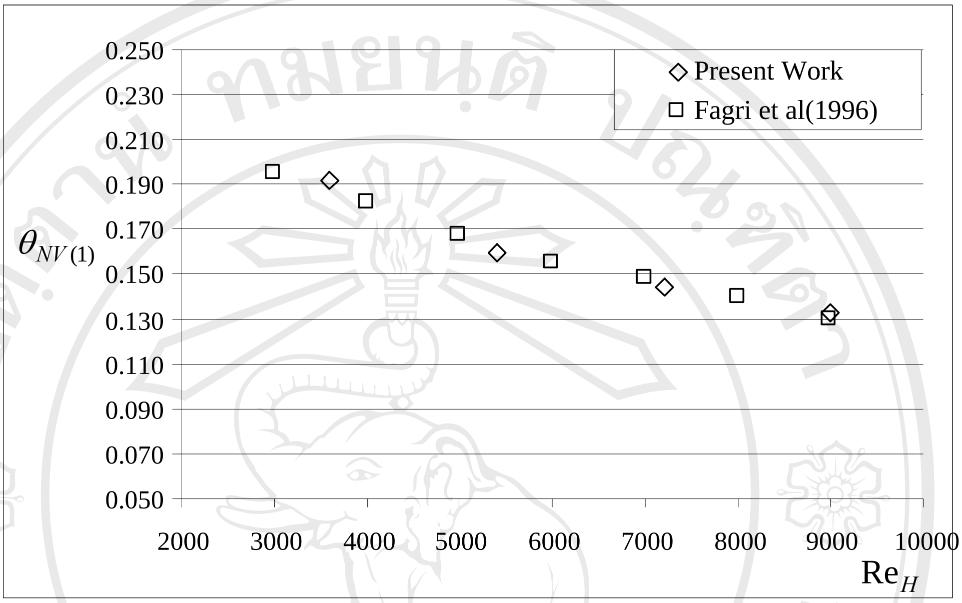

Figure 5.11 Thermal wake function for the first adiabatic module.
No vortex generator.

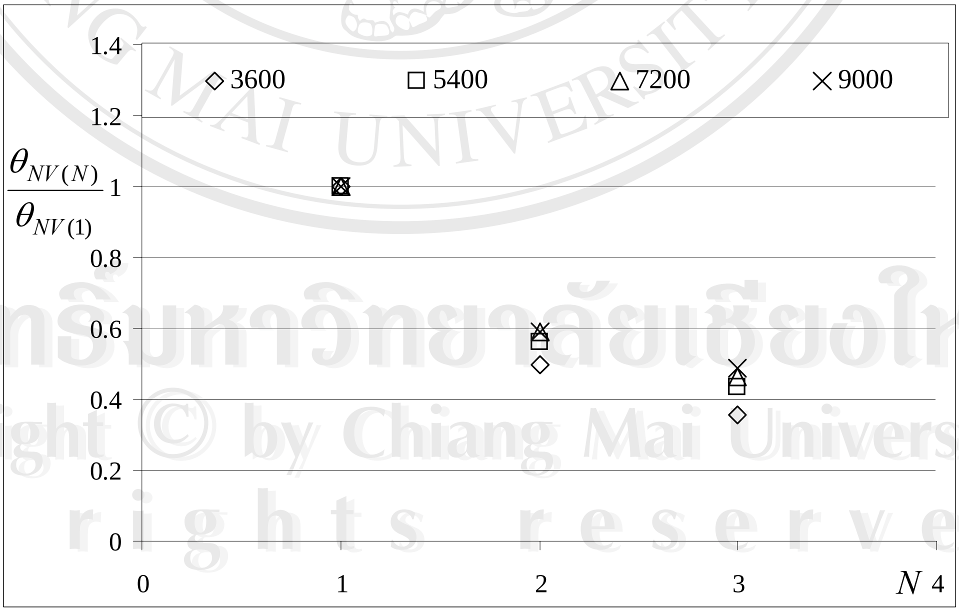

Figure 5.12 The thermal wake functions for other downstream modules.
No vortex generator.

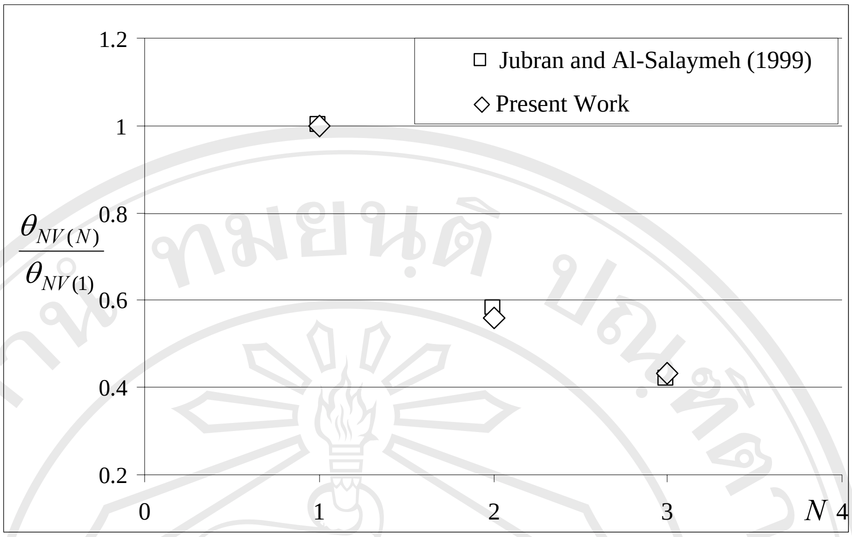

Figure 5.13 The thermal wake functions for other downstream modules compared with the data of Jubran and Al-Salaymeh(1999). No vortex generator.

(b) With vortex generators

Figures 5.14 and 5.15 show the thermal wake functions of the modules when there is a set of vortex generator installed in front of all modules. It could be seen that the technique could reduce the thermal wake function effectively due to the continuous longitudinal vortices promotion by the vortex generators. In this case higher the attack angle results in more reduction of the thermal wake function.

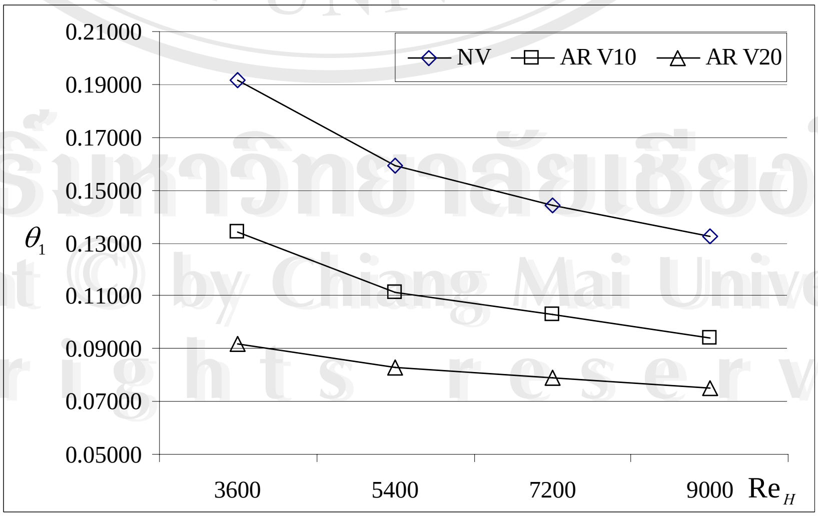

Figure 5.14 Thermal wake function for the first adiabatic module. Vortex generators are integrated in front of all modules.

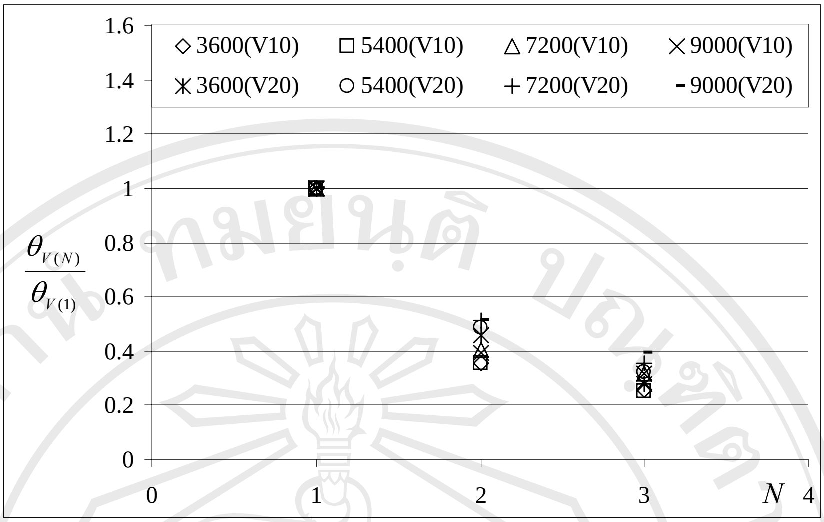

Figure 5.15 The thermal wake functions for other downstream modules. Vortex generators are integrated in front of all modules.

A correlation of the thermal wake function with the related parameters could be written in a form as

$$\frac{\theta_{V(N)}}{\theta_{V(1)}} = 0.26562\,\mathrm{Re}_H{}^{0.1472}\,N^{-1.0871}\tan\alpha^{0.11755} \qquad (5.12)$$

The correlation gives ± 15 % error from the experimental data.

To relate the equation of the modules having a set of vortex generators to that without the generators, a correlation of the thermal wake functions in the first row could be written in a form as

$$\frac{\theta_{V(1)}}{\theta_{NV(1)}} = 0.27435\,\mathrm{Re}_H{}^{0.09684}\tan^{0.2351} \qquad (5.13)$$

The correlation gives ± 5 % error from the experimental data. The results are also shown in Figure 5.16.

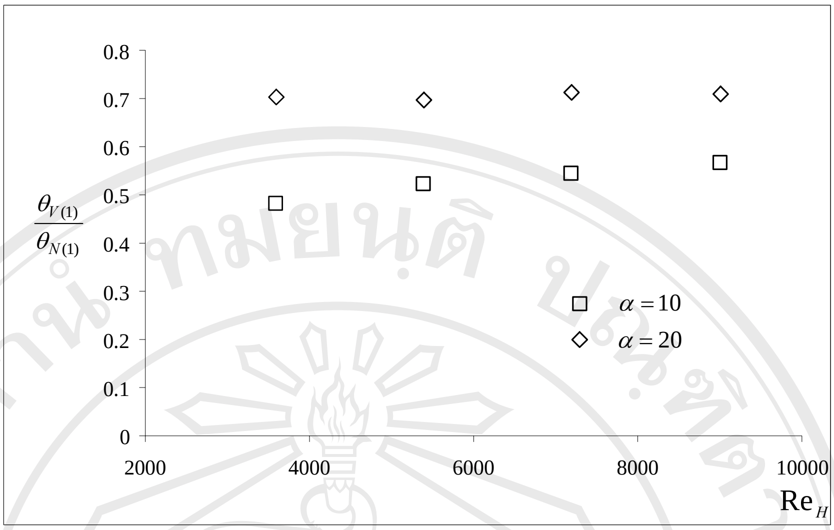

Figure 5.16 The ratio of thermal wake functions of the modules with and without vortex generator at the first row. The vortex generators are set in front of all modules.

The thermal wake function of the modules with integrated vortex generators could be evaluated from that without the vortex generator as

$$\frac{\theta_{V(N)}}{\theta_{NV(N)}} = \left(\frac{\theta_{V(N)}}{\theta_{V(1)}}\right) \times \left(\frac{\theta_{V(1)}}{\theta_{NV(1)}}\right) \times \left(\frac{\theta_{NV(1)}}{\theta_{NV(N)}}\right) \qquad (5.14)$$

5.1.4.3 Module Temperatures

Figure 5.17 shows the average module temperature in each row when there is no vortex generator and Figure 5.18 gives the value when the vortex generators are integrated to the module array at the attack angle of 20^{o}. The values of C_x and C_y are 19 and 18 mm, respectively. It could be seen that for the latter case, the module temperatures are less than those without the devices, significantly. The calculating results of the module temperatures from the technique described agree very well with those of the measuring data in both cases.

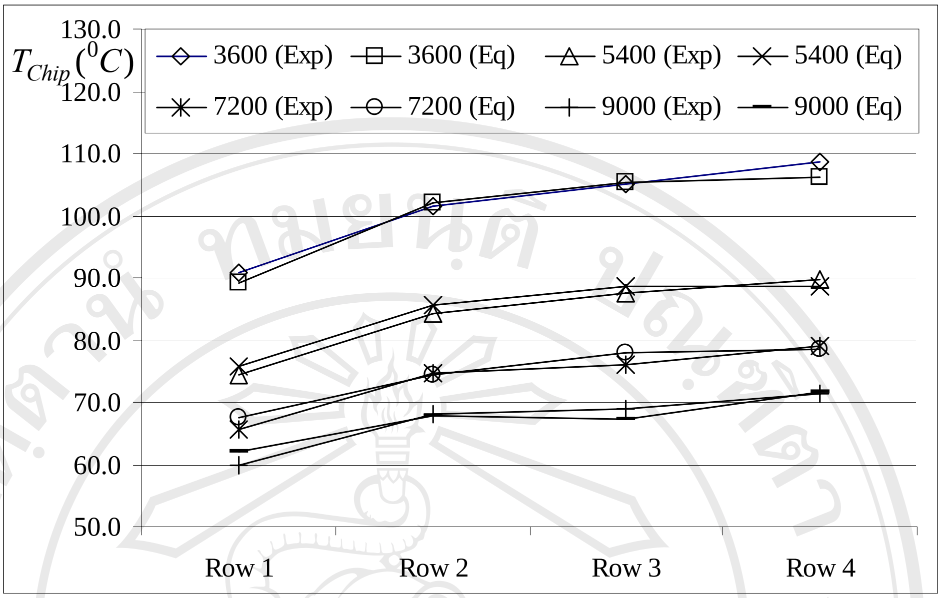

Figure 5.17 The average modules temperature when there is no vortex generator.

(The average temperature in each row has a maximum uncertainty of 5 %).

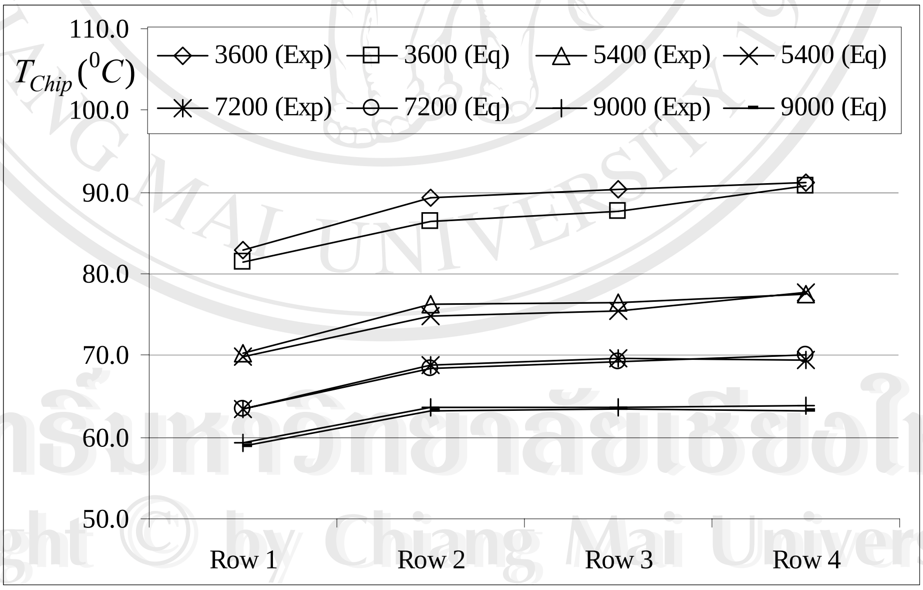

Figure 5.18 The modules temperature when the vortex generators are integrated.

(The average temperature in each row has a maximum uncertainty of 7 %).

5.1.4.4 Pressure Drop

When there are vortex generators integrated in front of all electronic modules, higher pressure drop in the fluid flow is obtained as shown in Figure 5.19. Higher the attack angle also results in the higher pressure drop.

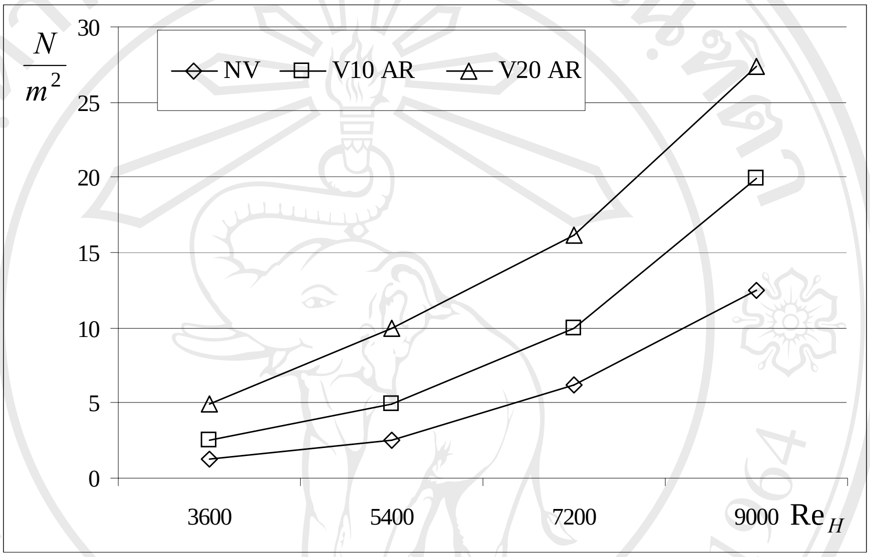

Figure 5.19 The pressure drop in air flow.

5.4.2 Staggered Array

5.4.2.1 Adiabatic Heat Transfer Coefficient

(a) No vortex generator

Figure 5.20 shows the adiabatic heat transfer coefficient in term of Nusselt number($Nu_{NV} = \frac{h_{ad} L_X}{k}$) at different module positions and Reynolds number($\mathrm{Re} = \frac{V(2H)}{\nu}$) when there is no vortex generator. The heat transfer coefficient in term of Nusselt number is the highest at the first row and the values in rows 2 and 3 slightly drop due to the flow blockage of the consecutive module which creates a flow recirculation between the modules (Meinders and Hanjalic, 2002). The data in rows 3 and 4 are nearly constant which means that around this region the fully developed flow occurs. The heat transfer coefficient in the 5^{th} module also increases since the air could flow through the module more freely and the result at this module is not taken in account.

Wirtz and Colban(1996) gave an experimental value of channel Nusselt number with channel Reynolds number in fully developed region. It could also be seen that our experiments at the 4^{th} row also agree very well with the data of Wirtz and Colban(1996) in the fully developed region. The comparison is shown in Figure 5.21.

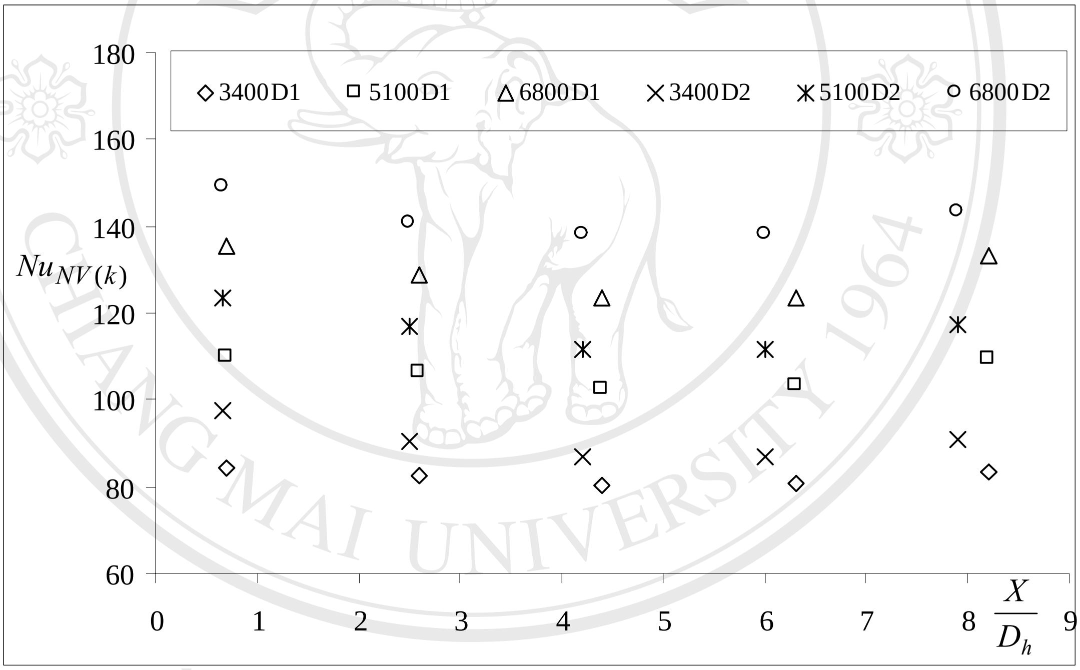

Figure 5.20 The adiabatic heat transfer coefficient in term of Nusselt number at different positions of the chip modules and Reynolds number. No vortex generator.

At fully developed flow region (the 4^{th} module), the fully developed Nusselt number ($Nu_{(NV)fd}$) could be correlated as

$$Nu_{(NV)fd} = 0.078776 \, \mathrm{Re}_H^{0.76475} \, D^{-0.16295} \left(\frac{H}{L_X} \right)^{-0.43104} \qquad (5.15)$$

The correlation gives ± 7 % error from the experimental data.

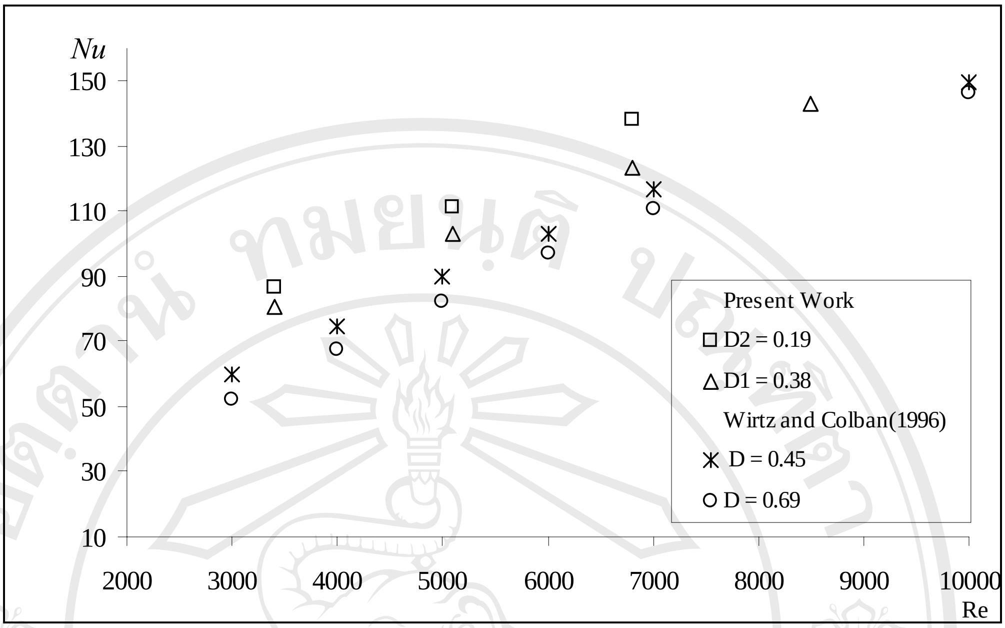

Figure 5.21 The value of $Nu = \frac{h_{ad} L_X}{k}$ at fully developed region with $\mathrm{Re}_H = \frac{V(2H)}{\upsilon}$ in case of staggered module array(Wirtz and Colban, 1996). No vortex generator.

Figure 5.22 gives the ratio of the Nusselt number at any position with the fully developed Nusselt number (Nu/Nu_{fd}).

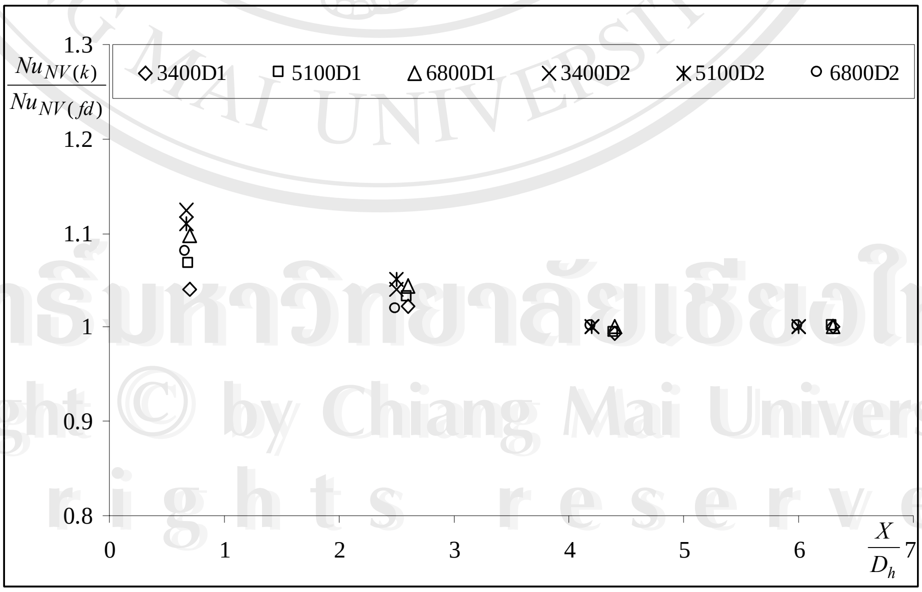

Figure 5.22 The ratio of the Nusselt number at any position with the fully developed Nusselt number at different Reynolds number.

From the figure, the ratio for the entrance region (rows 1-4) could also be correlated with the related parameters as

$$\frac{Nu_{NV(k)}}{Nu_{NV(fd)}} = 1.0205\,\mathrm{Re}_H^{\;0.0036243}\left(\frac{X}{D_h}\right)^{-0.040368} D^{-0.01233} \tag{5.16}$$

The correlation gives ± 5 % error from the experimental data.

Figure 5.23 also shows the value of the Nusselt number at various positions compared with that at the first row when there is no vortex generator integrated.

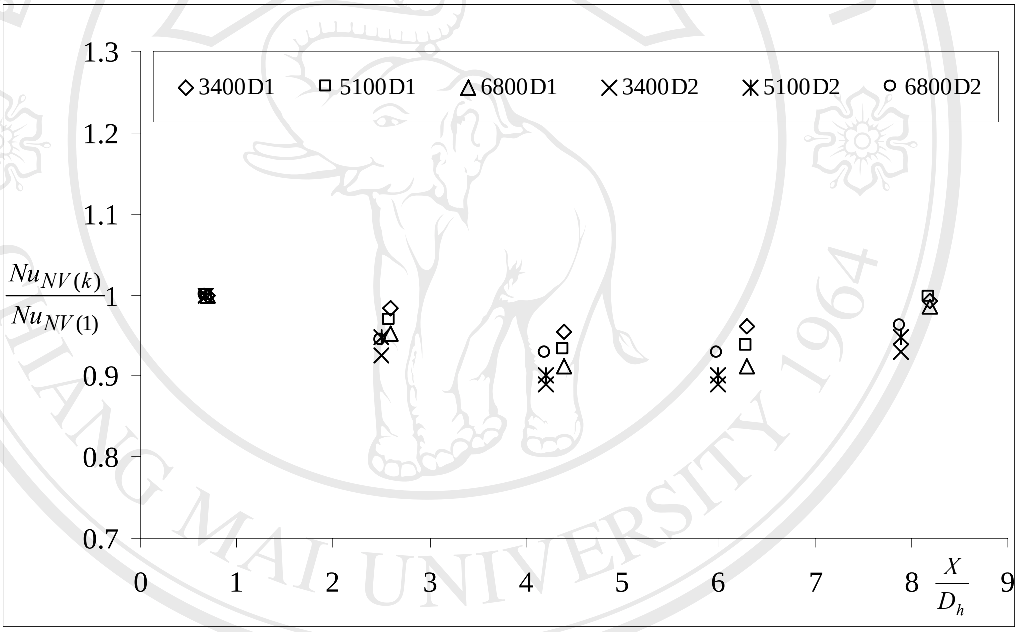

Figure 5.23 The ratio of adiabatic Nusselt number at different positions to that at the first row at various values of $\frac{X}{D_h}$. No vortex generator.

From the figure, it could be seen that the value of Reynolds number slightly affect on the ratio of the Nusselt number at different positions to that at the first row. For the fully developed region (row 1 to row 4), a correlation could be performed as

$$\frac{Nu_{NV(k)}}{Nu_{NV(1)}} = 1.034\,\mathrm{Re}_H^{-0.00008732}\left(\frac{X}{D_h}\right)^{-0.024322} D^{0.041869} \tag{5.17}$$

The correlation gives ± 4 % error from the experimental data.

(b) With vortex generators

In this case, only a winglet is used to generate vortex for each module since a set of winglet pairs will block the air flow in the staggered arrangement.

Figure 5.24 shows the adiabatic heat transfer coefficients when there are vortex generators integrated in front of all chip modules. Since the longitudinal vortices are performed in the fluid flow by the vortex generators then the heat transfer coefficients in all rows could be increased more than the previous case, especially at the second and the third rows. The Reynolds number does not give a strong effect to the heat transfer augmentation. The angle is not recommended to be over 20^o because it will block the flow and create high pressure drop. The density of the modules does not give a strong effect on the ratio of Nusselt number.

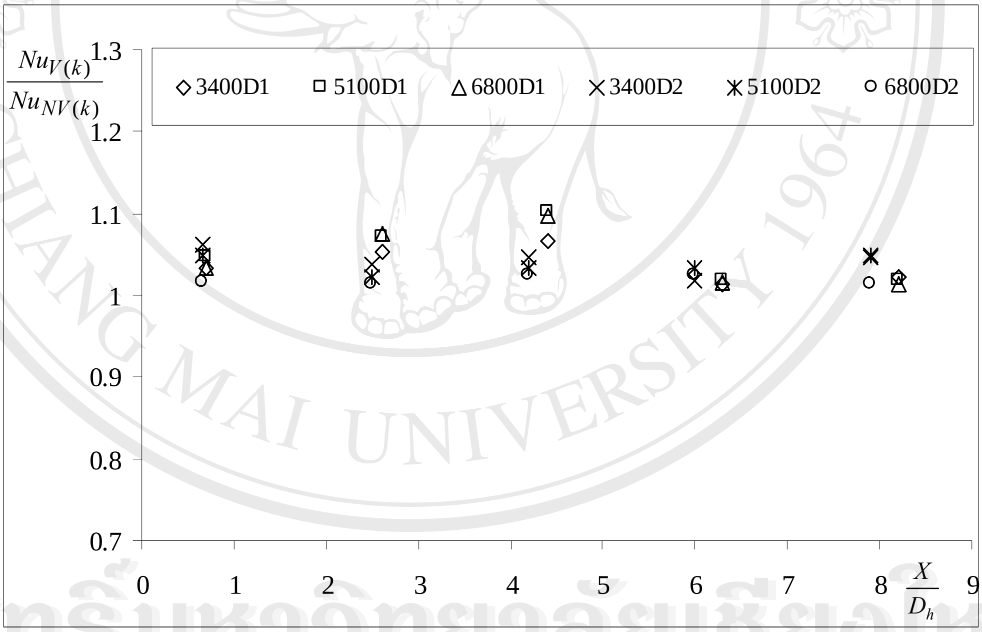

Figure 5.24 The heat transfer enhancement in term of Nusselt numbers with and without vortex generators. The vortex generators are integrated in front of all modules. The attack angle is 20 degree.

Figure 5.25 shows the ratio of adiabatic Nusselt numbers at different positions and different attack angles with that at the first row. The parameters could be correlated as

$$\frac{Nu_{(V)}(k)}{Nu_{(V)}(1)} = 0.88637\,\mathrm{Re}^{0.022374}\left(\frac{X}{D_h}\right)^{-0.029147} D^{0.064962} \qquad (5.18)$$

The correlation gives ± 7 % error from the experimental data.

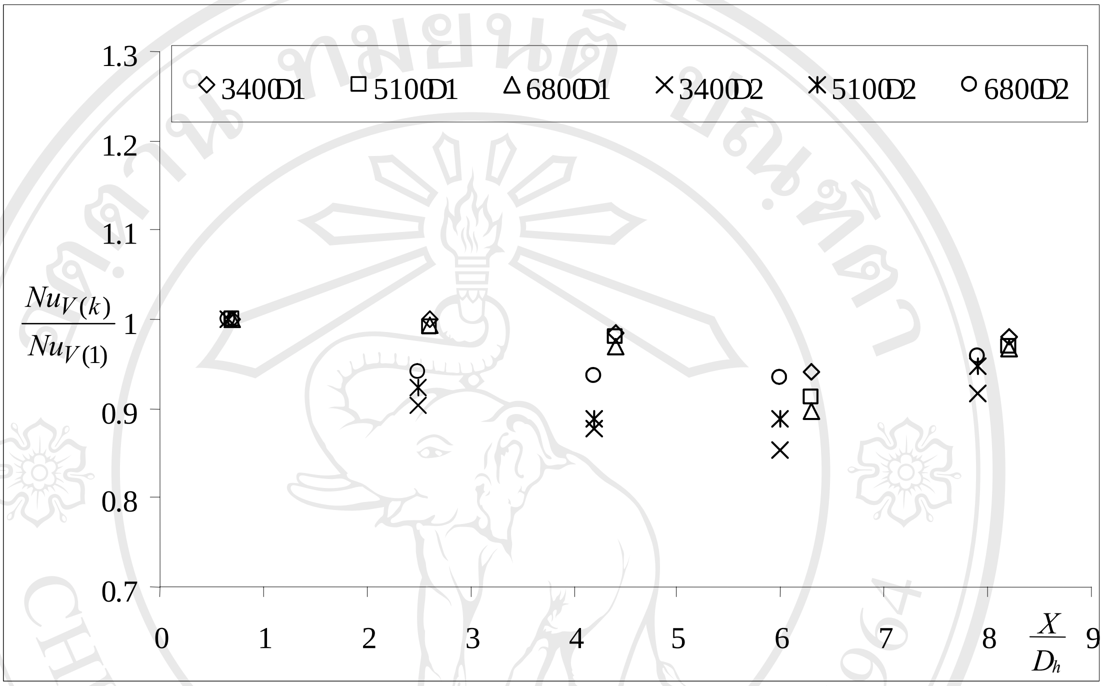

Figure 5.25 The ratio of adiabatic Nusselt numbers at different positions to that at the first row at various values of $\frac{X}{D_h}$. There is a set of vortex generators integrated in front of all modules.

A correlation between the Nusselt numbers in the first row (with and without vortex generator) and Reynolds number is given as

$$\frac{Nu_{V(1)}}{Nu_{NV(1)}} = 1.339\,\mathrm{Re}_H^{-0.030728}\, D^{-0.0057923} \qquad (5.19)$$

The correlation gives ± 2 % from the experimental data. The results are also given in Fig. 5.26

From the above correlations, the adiabatic Nusselt number of the modules with integrated vortex generators could be evaluated from that without the vortex generator as

$$\frac{Nu_{V(k)}}{Nu_{NV(k)}} = \left(\frac{Nu_{V(k)}}{Nu_{V(1)}}\right) \times \left(\frac{Nu_{V(1)}}{Nu_{NV(1)}}\right) \times \left(\frac{Nu_{NV(1)}}{Nu_{NV(k)}}\right) \tag{5.20}$$

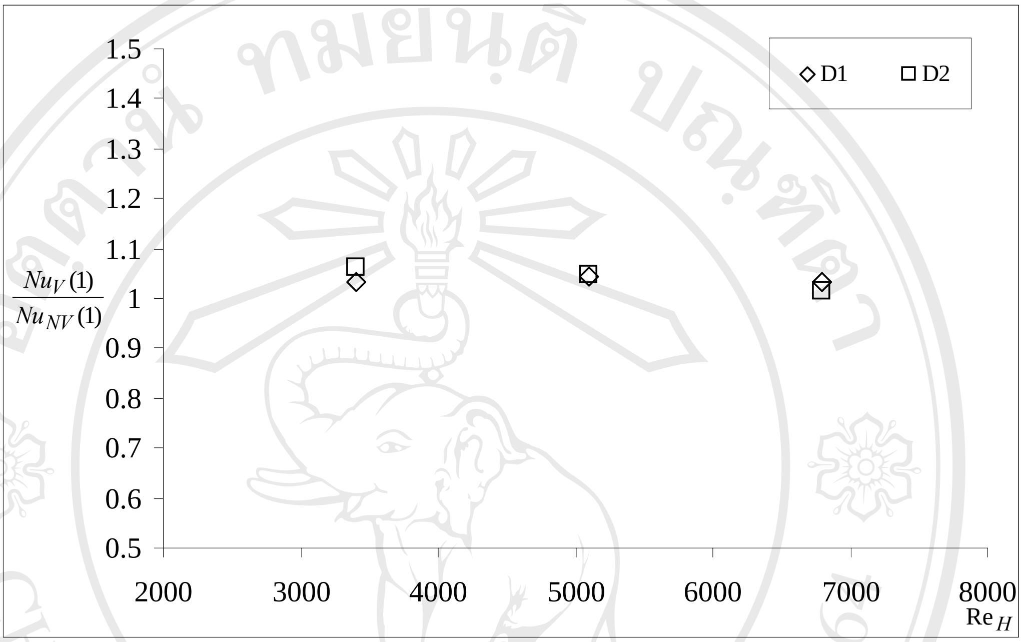

Figure 5.26 The ratio of adiabatic Nusselt numbers with and without vortex generator for the first row at various values of Reynolds number. There is a set of vortex generators integrated in front of all modules.

5.4.2.2 Thermal Wake Function

(a) No vortex generator

Figure 5.27 shows the results of thermal wake function of the module immediately downstream from the heating module when there is no vortex generator. It could be seen that the thermal wake function of the modules set in-line with the heating element has a significant value compared with that of the misaligned modules. The correlation of the thermal wake function could be

$$\theta_{IN,NV(N)} = 0.36708\,\mathrm{Re}_H^{-0.10762}\,N^{-0.84855} \tag{5.21}$$

and

$$\theta_{MN,NV(N)} = \theta_{IN,NV(N)} - 0.078107\,\mathrm{Re}_H^{-0.0044852}\left(\frac{C_{yy}}{L_y}\right)^{1.1157} N^{-1.1160} \quad (5.22)$$

The correlation gives ± 15 % error from the experimental data.

where $\theta_{IN,NV(N)}$ and $\theta_{MN,NV(N)}$ are the thermal wake functions of the in-line and misaligned modules. C_{yy} is the spacing of the module from the heating module in y direction.

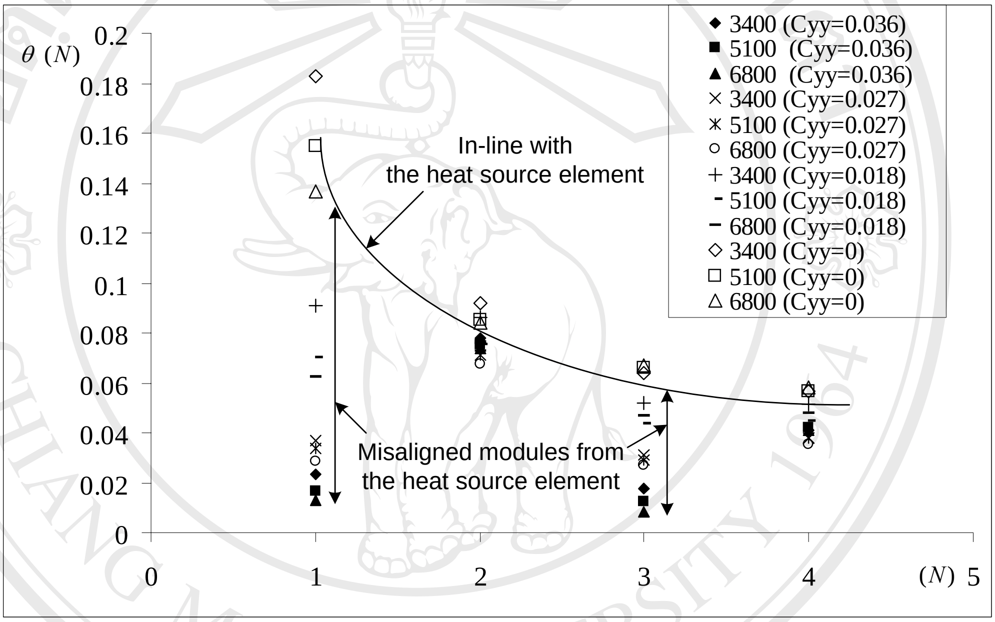

Figure 5.27 Thermal wake function for the first adiabatic module.
No vortex generator.

(b) With vortex generators

Figure 5.28 shows the thermal wake functions of the modules when there is a set of vortex generator installed in front of all modules. It could be seen that the technique could reduce the thermal wake function effectively due to the continuous longitudinal vortices promotion by the vortex generators.

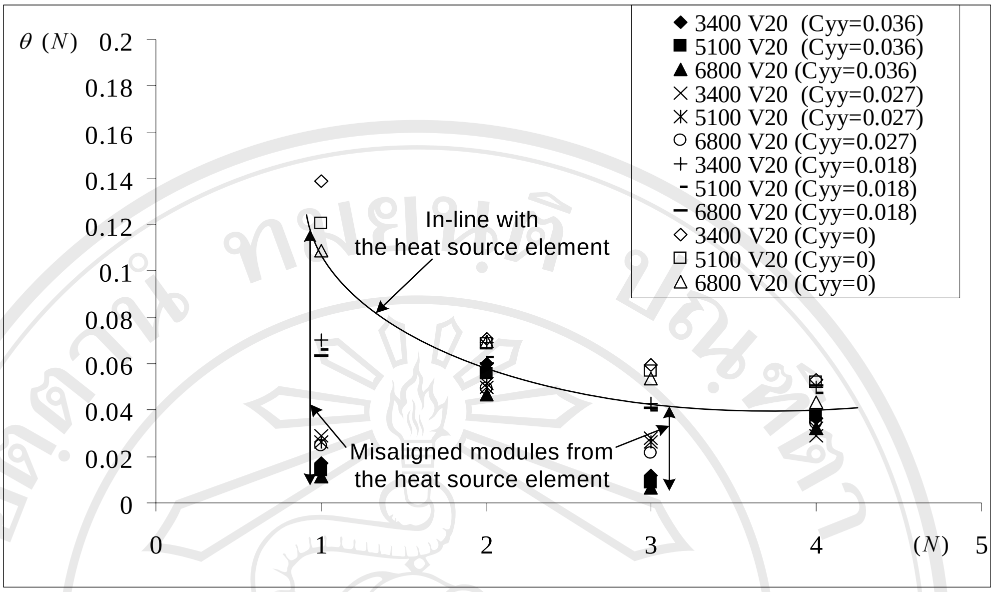

Figure 5.28 Thermal wake function for the first adiabatic module.
Vortex generators are integrated in front of all modules.

Similarly, a correlation of the thermal wake function with the related parameters could be written in a form as

$$\theta_{IN,V(N)} = 0.3672\,\mathrm{Re}_H^{-0.13879}\,N^{-0.60461} \qquad (5.23)$$

and $$\theta_{MN,V(N)} = \theta_{IN,V(N)} - 0.54463\,\mathrm{Re}_H^{-0.27758}\left(\frac{C_{yy}}{L_y}\right)^{1.3073} N^{-0.96804} \qquad (5.24)$$

The correlation gives ± 15 % error from the experimental data.

5.4.2.3 Module Temperatures

Figure 5.29 shows the average module temperature in each row when there is no vortex generator and Figure 5.30 gives the value when the vortex generators are integrated to the module array at the attack angle of 20°. The values of C_x, C_y and C_{yy} are 19, 18 and 18mm, respectively. It could be seen that for the latter case, the module temperatures are less than those without the devices, significantly. The calculating results of the module temperatures from the technique described agree very well with those of the measuring data in both cases.

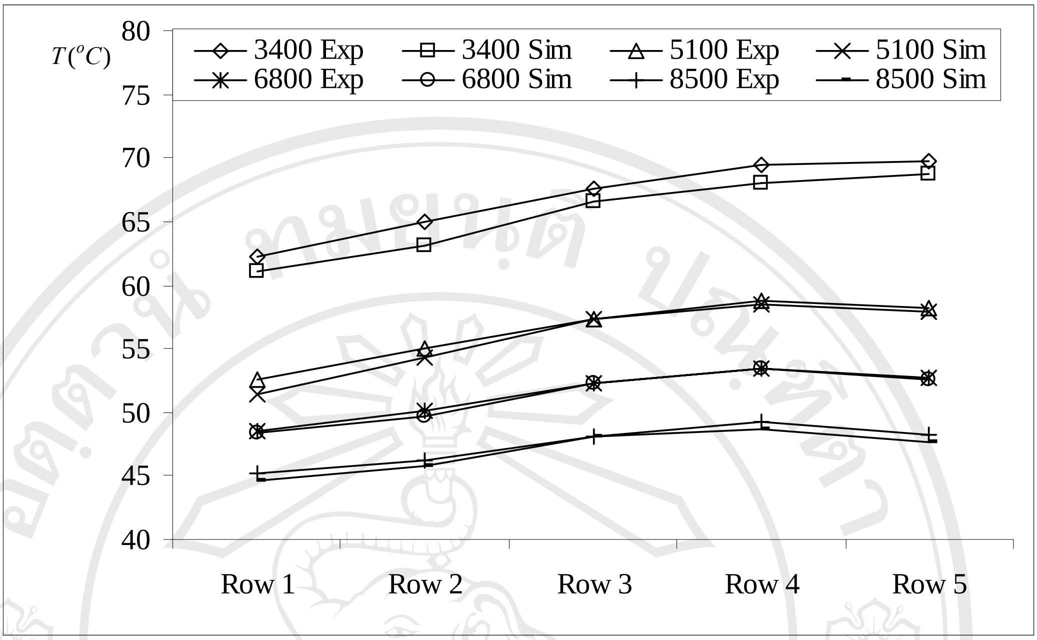

Figure 5.29 The average modules temperature when there is no vortex generator.(The average temperature in each row has a maximum uncertainty of 7 %).

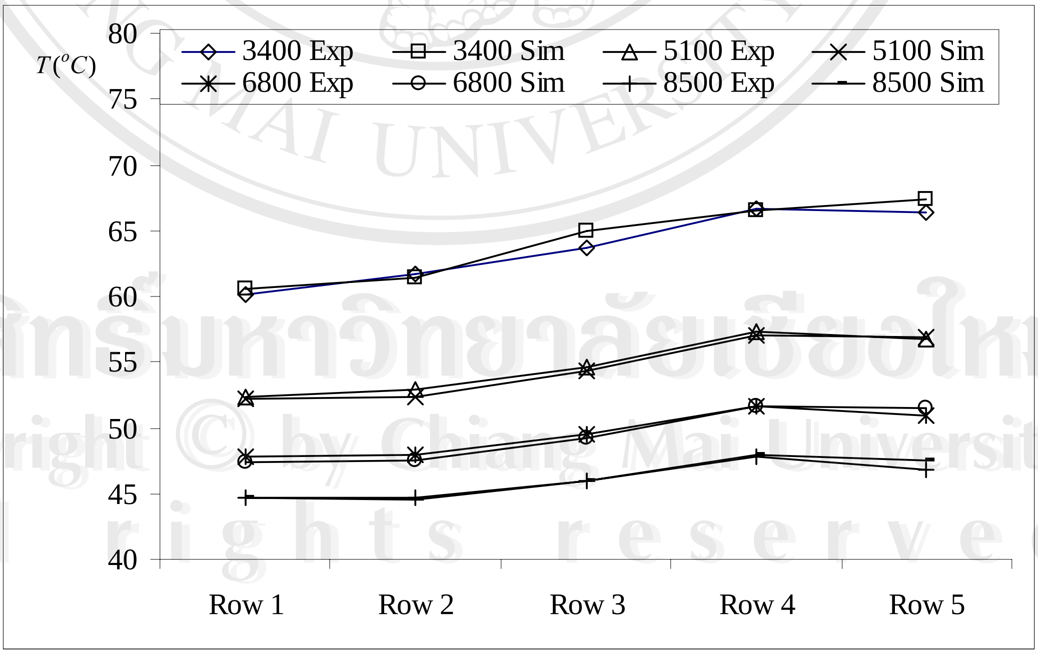

Figure 5.30 The modules temperature when the vortex generators are integrated. (The average temperature in each row has a maximum uncertainty of 4 %).

5.4.2.4 Pressure Drop

When there are vortex generators integrated in front of all electronic modules, higher pressure drop in the fluid flow is obtained as shown in Figure 5.31. However, the values are less than those of the in-line array in the previous case.

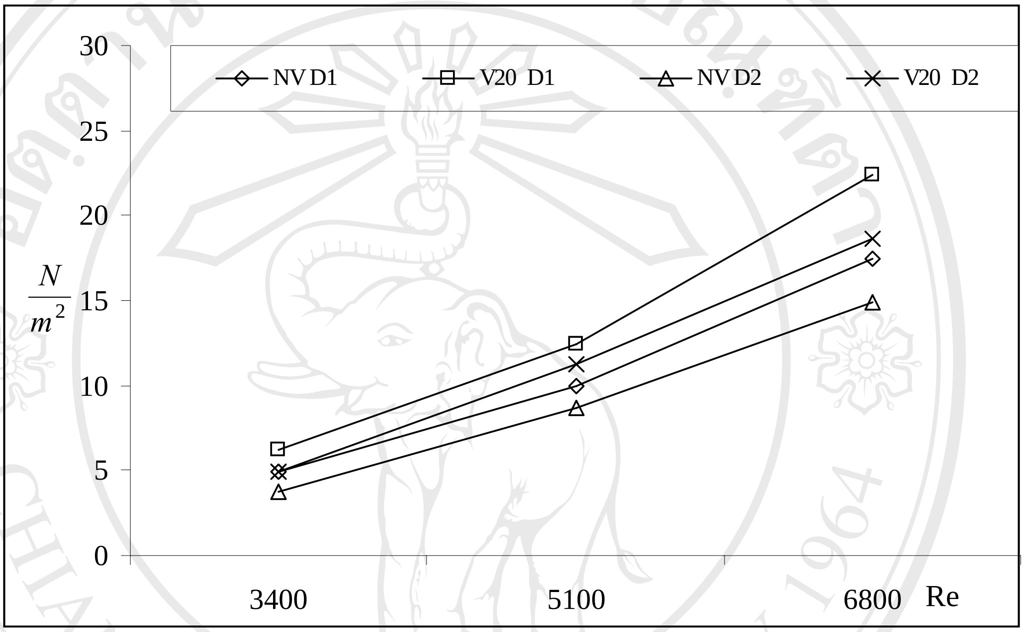

Figure 5.31 The pressure drop in air flow.

5.5 Conclusion

From the study, it could be concluded that

1. The delta winglet vortex generators could enhance the adiabatic heat transfer coefficient and reduce the thermal wake function effectively both in-line and staggered arrays. More attack angle results in higher heat transfer augmentation and also the pressure drop in the fluid flow.
2. In case of setting the vortex generators in front of the first row only, the heat transfer enhancement is significant only the first row.
3. The superposition method with the heat transfer models developed could be used to predict the module temperatures very well for both in-line and staggered arrays.